The
Mars Observer Laser Altimeter
Laser Transmitter

Robert S. Afzal

Code 924

NASA Goddard Space Flight Center

Greenbelt, MD 20771

(301) 286-5669

Abstract

The Mars Observer Laser Altimeter utilizes a space qualified diode laser pumped Q-switched Nd:YAG laser transmitter. A simple numerical model of the laser energetic is presented, which predicts the pulse energy and width compared to the available data. The temperature dependence is also predicted. This is particularly important in determining the operational temperature range of the transmitter especially for a passive thermally controlled laser operating in the space environment.

Key Words: Diode Pumped, Solid State Laser, Space Qualified

Introduction

The Mars Observer Laser Altimeter[1] (MOLA) is one of seven instruments aboard the Mars Observer spacecraft launched on September 25, 1992. MOLA'S primary mission is to gather Martian topographic data on a 0.2° x 0.2° grid with 30 m vertical accuracy and short baseline (≈ 100 km) topographic profiles with a 2 m vertical accuracy. The MOLA laser transmitter utilizes a diode laser pumped Nd:YAG laser which to our knowledge is the first diode laser pumped solid state laser to operate in space. The mission specifications and constraints of space qualification, which are mission specific, place strict requirements on the design and operation of the laser. Some of the environmental conditions that the instrument must survive uncompromised are, launch vibrations both random and sinusoidal, pyrotechnic shock and launch sound levels. The instrument capabilities must not be degraded under the conditions of thermal cycling (between -5 and 40 C) and must withstand radiation dosages expected during the mission[2]. For this mission not only does the laser transmitter (LT) need to survive launch and the journey to Mars, but had to meet the specifications summarized in Table 1. The laser is required to deliver 35 mJ pulses through 0.6 billion shots (≈ 2 Earth years - 1 Martian year). Although a laser can be built in the laboratory to meet performance specifications relatively routinely, the mission constraints demand uique options and compromises to be made in the materials used and the design in order to ensure the success of the mission. Further constraints, perhaps even more demanding, were those of cost and delivery time. This paper describes the MOLA laser and presents a simple model predicting the operational behavior of the laser based on the available test results.

Description of the laser

The MOLA laser transmitter was designed and built[3] by McDonnell-Douglas Electronic Systems Co. in St. Louis, MO. The LT was designed to be a Q-switched diode laser pumped Nd:YAG laser because the all solid state system was the most promising technology for a light weight, rugged and efficient laser transmitter. At the heart of the MOLA LT is a diode laser pumped slab of Cr:Nd:YAG within a Q-switched crossed Porro resonator. Although crossed Porro resonators introduce a lot of intracavity loss, they are much more insensitive to movement of cavity elements compared to conventional mirror resonators thereby ensuring a higher probability of surviving launch without misalignment. Figure 1 shows a schematic of the laser. A slab of 1% doped Nd:YAG was codoped with 0.05% Cr for purposes of radiation hardening. The nine bounce Brewster cut zig-zag slab was cut with a 3.4 x 3.4 mm cross section with, 5.7 x 4.6 cm major and minor lengths. Thermal and gain inhomogeneities within the slab are compensated to 1st order by image inversion off of each bounce inside the slab. 4 stacks of 11 diode laser bars side pump the slab and the opposite slab face is aluminum coated to reflect the unabsorbed pump light back into the crystal. The 4 diode stacks are pulsed at 10 Hz for a duration of 150 μs with a peak output power of 1760 watts at room temperature.

The slab is placed within a crossed Porro "z" resonator. The two prisms are parallel to each other but offset by 45° in azimuthal angle from the slab axis. Therefore the Porro prisms are crossed when viewed through the image inverting slab. Alignment of the laser beam in the sensitive direction of each Porro prism is accomplished by intracavity Risley wedges. A LiNb03 Q-switch is in one arm of the "z" with the gain medium in the other. A 0.57 λ wave plate compensates for depolarization in the Q-switch arm Porro prism. The wave

plate prism pair rotate the polarization 90° in a double pass creating a low Q resonator. 1/4 λ voltage applied on the Q-switch then creates the high Q condition. Output coupling is achieved by rotating a 1/4 λ plate in the gain arm of the "z" and coupling out the orthogonal polarization through one of the polarizing cubes. The lasers' optimal output coupling can then be empirically determined simply by rotating the 1/4 λ plate and maximizing the output power.

Description of the numerical model

We begin with the standard coupled ordinary differential equations describing the operation of a Q-switched laser[5,6]. The equations describe the action of two variables for inversion and photon densities starting from initial conditions with no driving terms. The Q-switch is modeled as a decaying exponential term in the dissipative cavity losses. The equations to be numerically integrated are:

$$\frac{dN}{dt} = -\gamma\sigma c N\phi \qquad (1)$$

$$\frac{d\phi}{dt} = \frac{2\sigma l N\phi}{t_r} - \frac{\phi}{t_c} \qquad (2)$$

where N is the inversion density and ϕ is the cavity photon number density.

All the work in making this model correspond to measured experimental data lies in an accurate determination of the initial conditions and a proper choice of the equation constants. The initial photon density is chosen to be 1 for simplicity. More accurately, the initial spontaneous fluorescence emitted into a solid angle subtended by the slab cross section at a distance of one cavity length should be used. This will only shift the position in time of the emergence of the laser pulse from the cavity and will not change the energy or pulsewidth. The initial inversion density was determined by considering

the total number of photons emitted from the diodes and absorbed by the slab that yielded a Nd ion in the excited state. The initial inversion was given by:

$$N_o = \frac{P t_p \alpha \xi \chi \eta}{V h \nu} \qquad (3)$$

where P = 1760 W is the peak diode pump power emitted by the stacks, tp = 150 μs the square pulse pump duration, a = 0.9 (typically) the double pass absorbed fraction, χ = 0.9 for a pump coupling efficiency, ξ = 0.965 for the quantum efficiency of the radiationless transfer from the pump level to the $4_F 3/2$ upper laser manifold[7], hv = 2.44 x 10-19 J for the photon energy and V = 0.59 cm3 the slab volume. Further reduction of the initial inversion density by spontaneous emission is accounted for by the factor[8]:

$$\eta = (1 - \exp(-t_p / t_{spon})) t_{spon} / t_P \qquad (4)$$

where tsp_{on} = 230 μs the spontaneous lifetime[5, 6] of Nd:YAG. In our case η = 0.737. We therefore started our equations with an initial inversion of ≈ 10^18 cm^-3.

Other equation constants used were as follows. t_r is the cavity optical round trip time which for a 37 cm long cavity is 2.47 ns. The nonuseful round-trip losses (nonoutput coupling) in the cavity were given by:

$$L = 2\alpha l + \ln(1 / \prod_i T_i^2) = 0.35 \qquad (5)$$

where al is the slab scattering losses and Ti is the transmission coefficient of the i^{th} element in the cavity. The Q-switch is then incorporated into the differential equations as an explicit time dependent loss term given by:

$$L(t) = L(1 + \exp(-t / \tau)) \qquad (6)$$

τ = 30 ns is the characteristic decay time of the Q-switch. The cavity decay time is then given by $t_c = t_r/(L(t) - \ln(R))$ where R is the effective output coupler reflectivity. Careful attention must be given to the value of the stimulated emission cross section because this number effects both the output energy and pulse width predictions. The cross-section used in this model was $\sigma = 2.8 \times 10^{-19}$ cm^2. There have been many values of σ published in the literature over the years. Based on two recent high quality determinations of the cross section[7,9] the value $\sigma = 2.8 \times 10^{-19}$ cm^2 was used. Since our pulse widths are $\approx 10^{-8}$ s $>> 10^{-11}$ s, the intramanifold Stark level thermalization time[10], we consider the 1.064 μm transition occurring from the $^4F_{3/2} \rightarrow {}^4I_{11/2}$ manifold not the R2 -> Y3 sublevels. Even though the sublevel cross section is 6.5×10^{-19} cm^2, in the long pulse regime the sublevels are in thermal equilibrium so we consider the manifold to manifold cross section which is 2.8×10^{-19} cm^2. In this regime the values of ref.7,9 agree. The value used for the 'inversion reduction factor'[5] is y = 1.2. Due to the rapid thermalization time, the $^4F_{3/2}$ doublet can be considered a single level. The equilibrium Boltzman distribution of the $^4I_{11/2}$ manifold places $\approx$ 20% of the atoms in the Y3 sublevel. Therefore for every dexcited atom there is only a reduction of $\approx$ 1.2 in the inversion. This value relies on a further assumption that the $4_1 11/2$ manifold relaxation time is long compared to the pulse width. If this were not true however, the maximum modification would be a reduction of y closer to unity. Given these parameters, the equations can be solved numerically to determine the time dependence of photon and inversion densities for different effective output coupler reflectivity's in order to obtain a value for R (see figure 2). This is necessary because output coupling in MOLA is achieved not through a fixed reflectivity but optimization through polarization induced losses. We used a standard Runge-Kutta fourth order technique to integrate the coupled differential

equations. The useful (emitted through the output coupler) photon density can be integrated to obtain the output pulse energy. The laser is multimode with the whole slab cross-section available for lasing, resulting in a near unity fill factor of the slab in calculating the pulse energy. It should be noted that although the zig-zag increases the optical length of the slab, for purposes of energy extraction (in the limit of gain saturation) the physical length of the slab is used. This is because in the regime of a near unity fill factor between laser mode and slab cross-sections, there is near unity overlap of the mode with itself off of each internal bounce within the slab thereby reducing the extracted energy per optical length. So for purposes of energy extraction, the slab can be considered as a straight pass not a zig-zag. Figure 3 compares the numerical model with the output pulse obtained from the LT.

Temperature Dependence

The temperature dependence of the LT is accounted for solely by the temperature dependence of the pump diodes. The first correction is a slight linear dependence on the output power with temperature given by P = 1800 - 4.4T where T is in “C and P is in watts. The second and more important effect of temperature is on the diode wavelength. Our model uses a 1 nm shift in wavelength for every 3.125 “C change in temperature.

The 44 diode bars are spread out in wavelength over 6 nm at a nominal temperature of 20 “C. The percent absorption of each bar was determined by considering the overlap of the bar’s wavelength and the Nd:YAG absorption spectra. See figure 4. An ensemble absorbed fraction of the total power was calculated by summing over the 44 bars. That fraction of total absorbed power was then calculated for every 3.125 “C change in temperature from 9° to 38°C. An eighth order polynomial fit to the data provides a continuous dependence of the total fraction of absorbed pump energy on temperature over the region

9° to 38° (see figure 5). That fraction is then used in equation (3) for a. The temperature dependence is therefore incorporated directly into the initial conditions of the system. It should be noted that although the diode bars are distributed in wavelength thereby decreasing the maximum output energy, the LT can operate over a much broader temperature range because there will always be some diodes overlapped with the peak absorption of Nd^{3+} in the temperature range of 9° to 38° C. The LT was required to be operational within this temperature range. Figure 6 compares the predicted and measured temperature behavior of the LT. By choosing various diode bar wavelength combinations the operational temperature range can be directly tailored to operate over different temperature regions expected by the instrument. In an all passively cooled instrument where a precise prediction of the instrument temperature is difficult to make, the operational temperature range of the laser can be the most critical engineering design point for the success of the mission.

Intracavity Fluence

An important consideration in the design and performance of the laser is the potential of damage to intracavity optical elements due to high fluences. It is therefore important to estimate the intracavity loading on each surface to determine the proximity to damage threshold. Based on our modeled results with an effective output coupler reflectivity of R = 0.4, we can construct a graphical representation of the two-way intracavity fluence circulating within the cavity to estimate the loading on all of the intracavity surfaces. Figure 7 shows the total energy on the Q-switch is ≈ 61 mJ. Given a mode size of ≈ 0.1 cm^2 and a pulsewidth of 7.2 nS, the average intensity on the Q-switch face is ≈ 85 Mw/cm^2. The MOLA LT mode however has a 2.4:1 peak to average ratio giving ≈ 200 Mw/cm^2. This is of some concern because the Q-switch has

survived 300 Mw/cm^2 under testing but not 400 Mw/cm2. It goes without saying that damage to the intracavity optics would severely compromise the performance of the LT. It is also clear from figure 7 that the design of the "z" resonator is such that the Q-switch arm has about half the fluence of the gain arm. The elements in the gain arm are less susceptible to damage and are at a lower level of concern.

Conclusions

We have presented a simple numerical model of the MOLA LT that predicts the output energy, pulse width and temperature dependence to better than 10% of the available experimental data. As with most models the largest sources of error come from experimental determination of the input parameters such as pump power and pump absorption and the accuracy of the equation constants. Even with a well studied material as Nd:YAG, there are still some uncertainties in the material parameters. Careful consideration must be given to the regime of application to be sure that the approximations made are still valid, due to this much better than 10% accuracy should not be expected at this level of treatment. It is interesting to note that it seems that the essential physics of this laser has been captured by this simple model without the need for a more detailed approach. This will now provide us with a powerful tool in the development of future diode laser pumped solid-state laser instruments.

RSA would like to thank MDESC. particularly Jeff Watts, as well as Jay Smith of NASA-GSFC for providing essential information and data of the MOLA LT and Todd Lang and Mark Selker of NASA-GSFC for helpful discussions.

References

1) M.T. Zuber, D.E. Smith, S.C. Solomon, D.O. Muhlman, J.W. Head, J.B. Garvin, J.B. Abshire, and J.L. Bufton; "The Mars observer Laser Altimeter Investigation", J. Geophys. Res., Vol. 97, No. E5, pp 7781-7797 (May 25, 1992).

2) The instrument had to withstand radiation dosages of over 100 KRad.

3) G. Gaither et al.; "Design of the Mars Observer Laser Altimeter Laser Transmitter," CLEO '91, Baltimore MD, Technical Digest, CF12, p 520

4) There are a number of treatments of crossed Porro resonators in the literature. One example is, M. Acherakar; "Derivation of Internal Incidence Angles and Coordinate Transformations Between Internal Reflections for Comer Reflectors at Normal Incidence", Opt. Engineer., Vol. 23, No. 5, pp 649. 674, (Sept/Ott 1984).

5) J.J. Degnan, "Theory of the Optimally Coupled Q-Switched Laser"; IEEE J. Quantum Electron., Vol. 25, No. 2, pp 214-220, (February 1989).

6) W. Koechner, Solid State Laser Engineering, New York: Springer-Verlag, 1976, ch. 8.

7) E.B. Treaty and Z. Lu, "Negative Lens Laser", SBIR Phase I final report, Candela Laser Corp., Wayland MA, Office of Naval Research Contract # N 00014-90-C-01 87, Arlington VA.

8) A.E. Siegman, Lasers, Mill Valley CA: University Science Books, 1986, ch 26.

9) W.F. Krupke, M.D. Shinn, J.E. Marion, J.A. Caird, and S.E. Stokowski; "Spectroscopic, Optical and Thermomechanical properties of Neodymium- and Chromium-Doped Gadolinium Scandium Gallium Garnet", J. Opt. Sot. Am. B, Vol. 3, No. 1, pp 102-113, (January 1986).

10) L.A. Riseberg and H.W. Moos, "Multiphonon Orbit-Lattice Relaxation of Excited States of Rare-Earth Ions in Crystals", Phys. Rev., Vol. 174, No. 2, pp429-

438, (Oct. 10, 1968) and W.M. Yen, W.C. Scott and A.L. Schawlow, "Phonon-Induced Relaxation in Excited Optical States of Trivalent Praseodymium in LaF3", Phys. Rev., Vol. 136, No. 1A, pp A271-A283, (Oct. 5,1964).

Table 1

	Weight	Available Power	Pulse Energy	Pulse Width	Repetition Rate	Lifetime
Specifications	6.26 Kg	14 W	40 ml	10 nS	10 Hz	6 X 108
Actual	5.38 Kg	13.7 w	41 mJ	7.6 nS	10 Hz	TBD

Figure Captions

1) Schematic of the MOLA laser.

2) Output energy (Triangles) and pulse width (circles) vs output coupling.

3) (a) Numerical simulation of the laser output pulse (photon density - solid line) and gain medium inversion density (dashed line). This case predicts a laser pulse of 46 mJ, 7.2 nS using R=O.4 output coupling and the diodes at 15 C. (b) Oscilloscope trace of the MOLA laser pulse of 44 mJ and FWHM = 7.6 nS.

4) Graph of Nd:YAG absorption spectrum around 0.8 μm also showing a representation of the number of diode bars (vertical columns) at each corresponding wavelength. The relative position of the bars and the Nd:YAG absorption is temperature dependent.

5) Graph of the calculated percentage of the total light emitted by the diodes absorbed by the slab as a function of temperature.

6) Graph showing the predicted pulse width (Solid circles), predicted pulse energy (solid triangles) and measured pulse energy (open squares) as a function of temperature.

7) Representation of the two-way circulating energy inside the MOLA laser cavity. Using the schematic of the resonator above, the intracavity energy can be estimated by trancing a vertical line from the element of interest, a Q-switch face for example, through the intersection of the two-way circulating energy curves. The total energy incident on that surface is the sum of the “forward” and “backward” values as read by the right-hand scale.

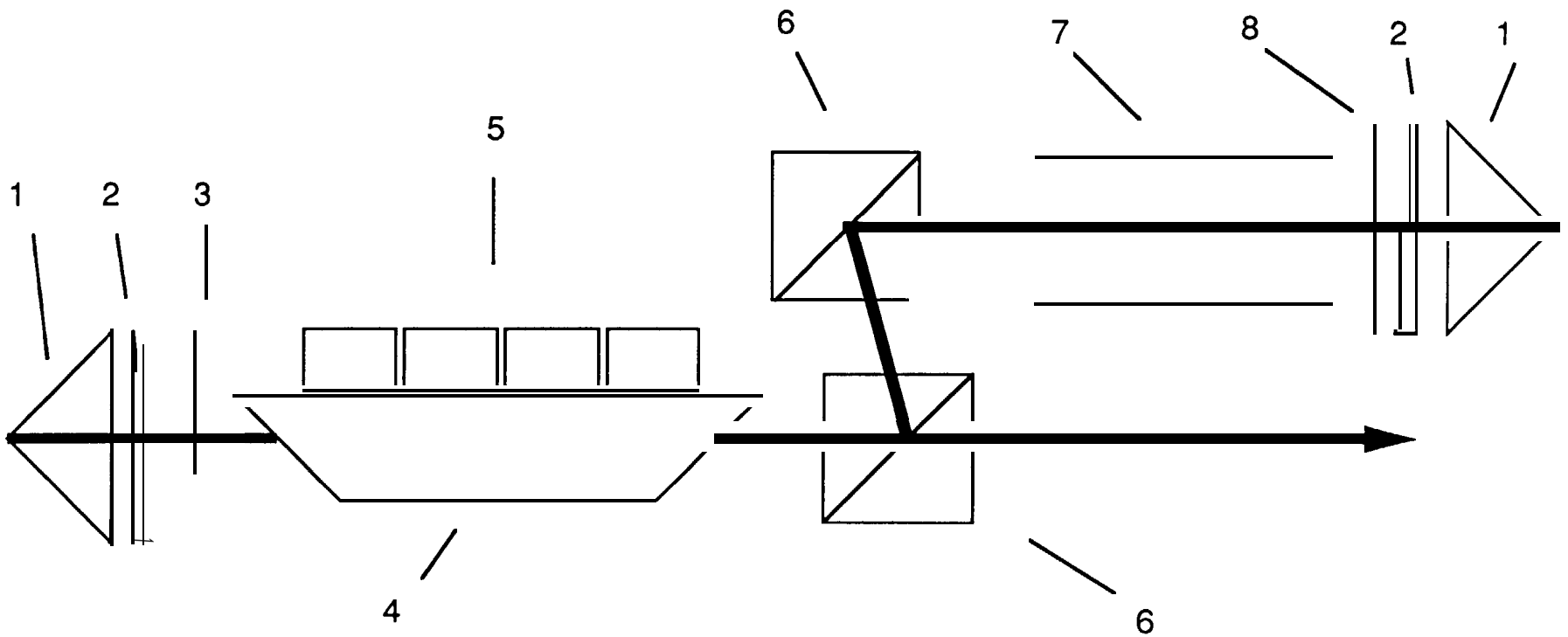

1- Porro Prism
2- Risley Wedge
3- 1/4 λ Plate
4 - Cr:Nd:YAG S ab
5 - Diode Laser Stacks
6- Polarizers
7 - Lithium Niobate Q-switch
8- 0.57 λ plate

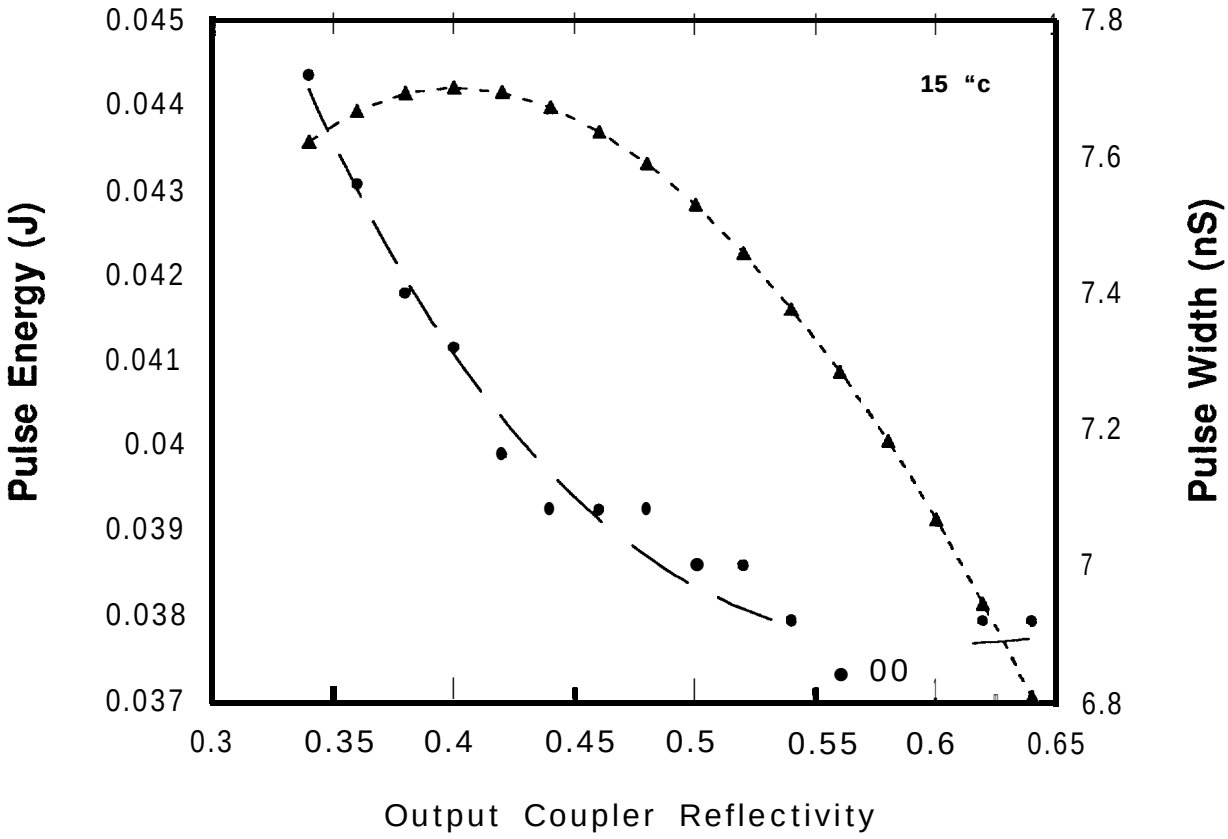
0.045
0.044
0.043
0.042
0.041
0.04
0.039
0.038
0.037
7.8
7.6
7.4
7.2
7
6.8
15 "c
00
0.3
0.35
0.4
0.45
0.5
0.55
0.6
0.65
Pulse Energy (J)
Pulse Width (nS)
Output Coupler Reflectivity

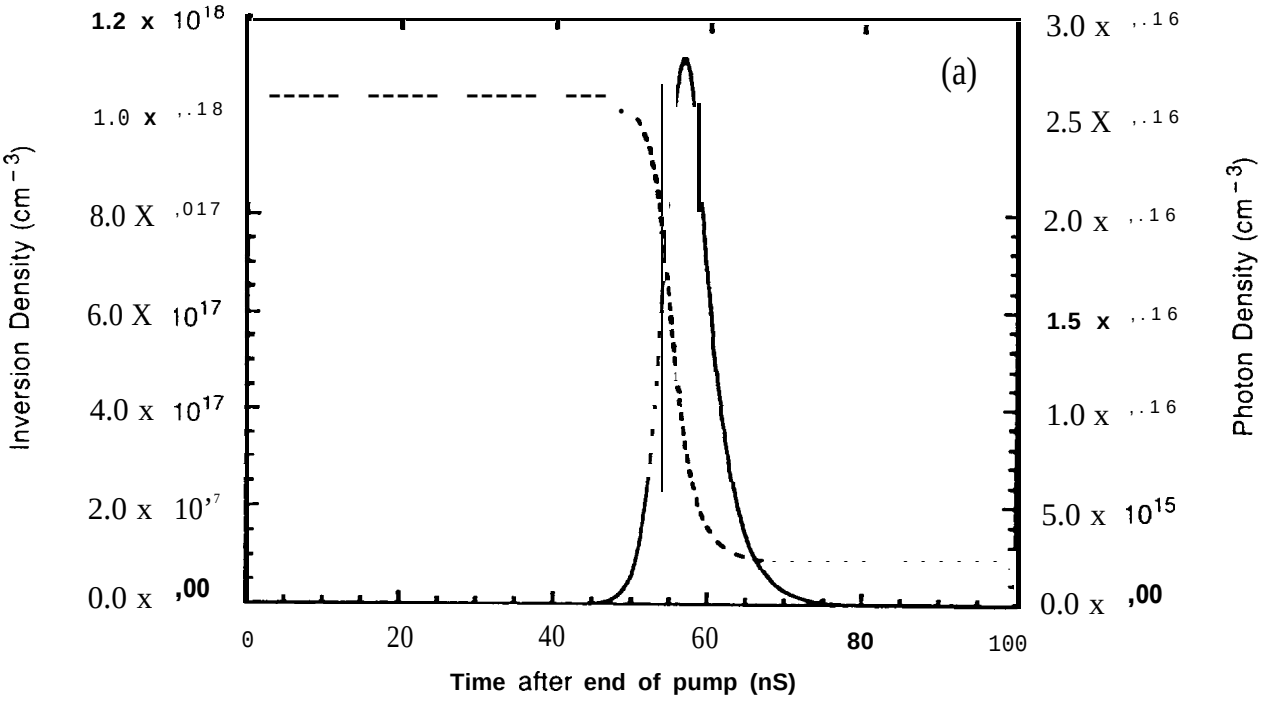
(a)
Inversion Density (cm⁻³)
Photon Density (cm⁻³)
1.2 x 10¹⁸
1.0 x
8.0 X
6.0 X 10¹⁷
4.0 x 10¹⁷
2.0 x
0.0 x
3.0 x
2.5 X
2.0 x
1.5 x
1.0 x
5.0 x 10¹⁵
0.0 x
0
20
40
60
80
100
Time after end of pump (nS)

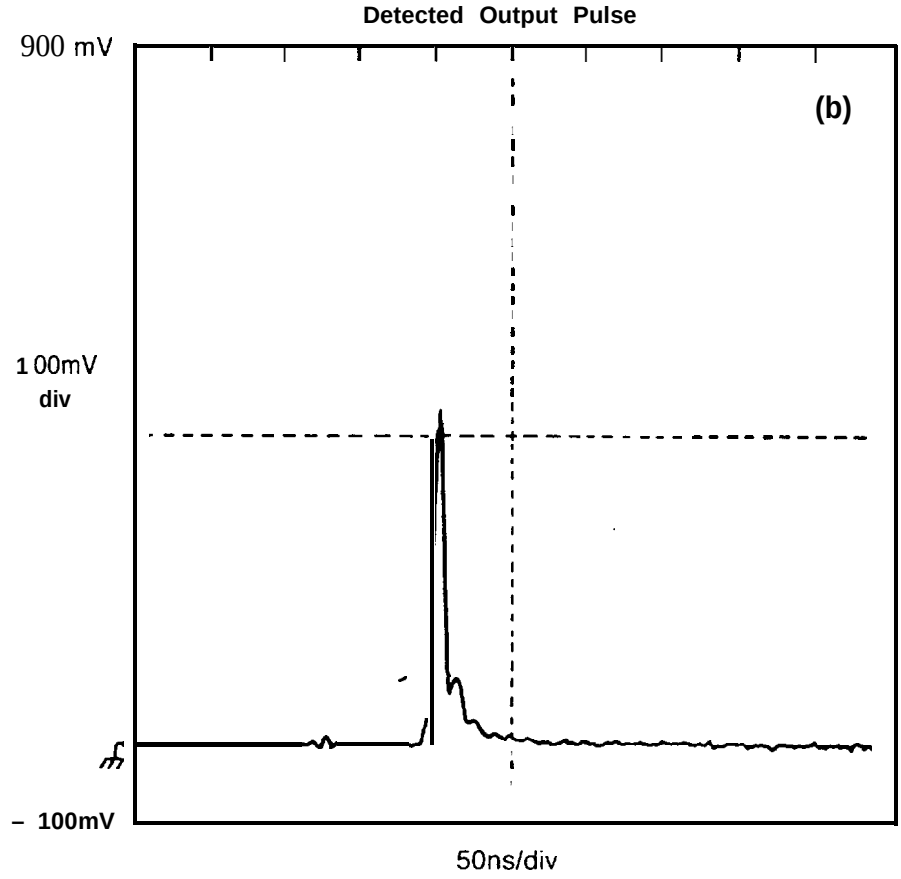
Detected Output Pulse
(b)
900 mV
100mV
div
– 100mV
50ns/div

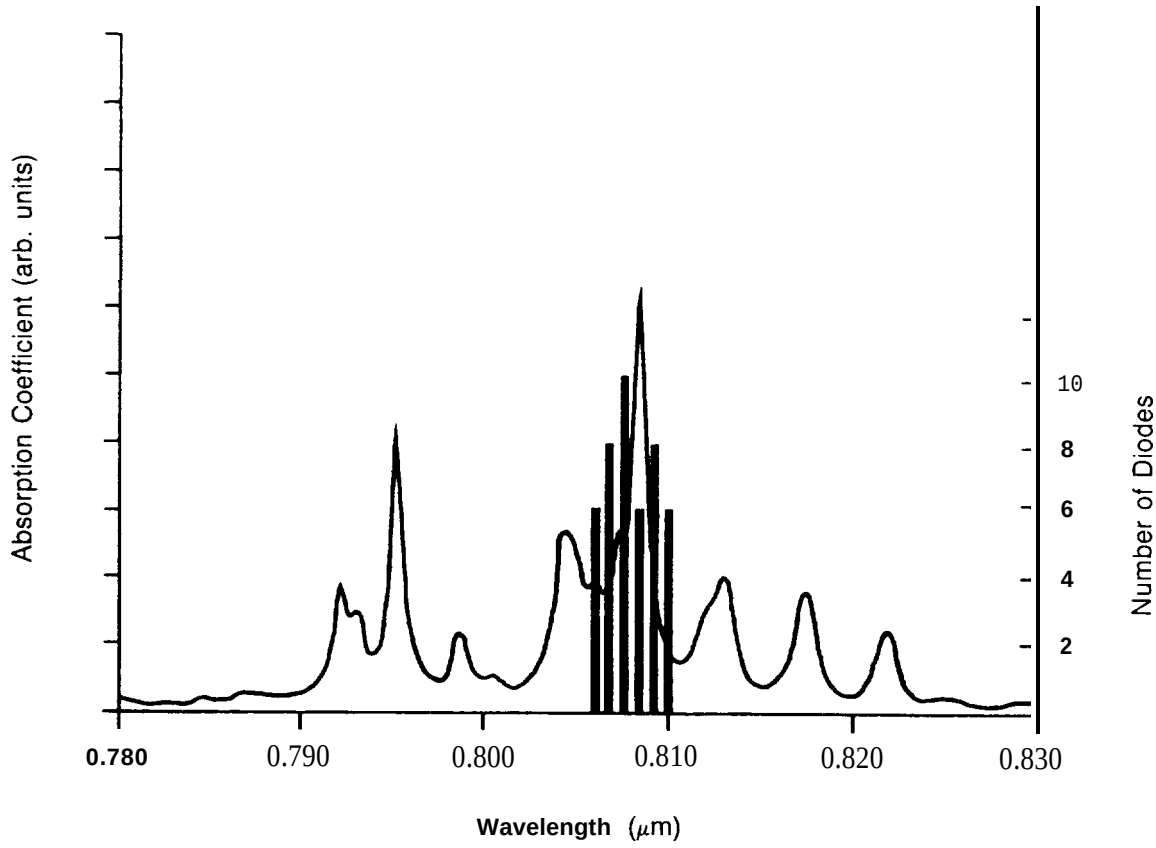
Absorption Coefficient (arb. units)
Number of Diodes
10
8
6
4
2
0.780
0.790
0.800
0.810
0.820
0.830
Wavelength (μm)

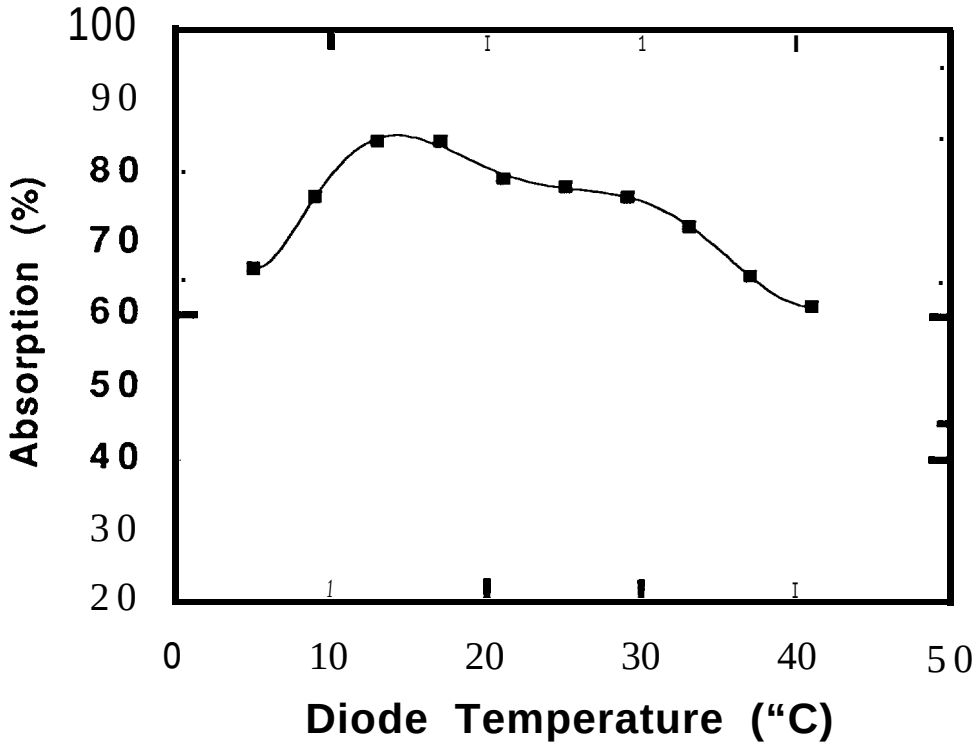
100
90
80
70
60
50
40
30
20
Absorption (%)
0
10
20
30
40
50
Diode Temperature (“C)

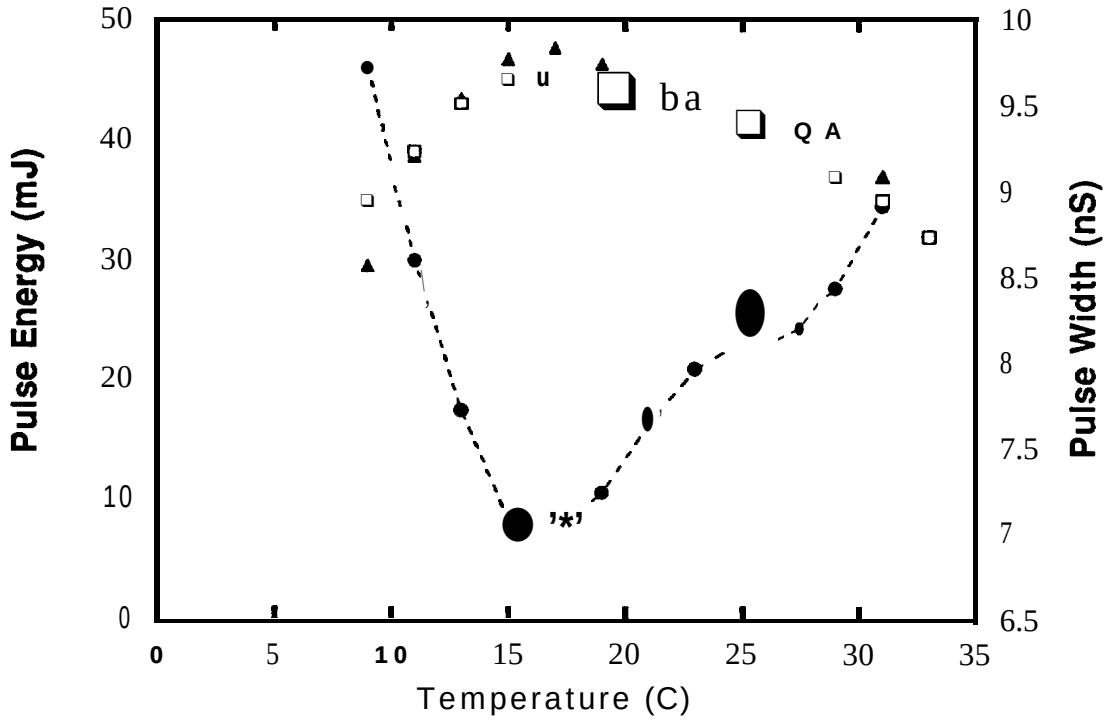
Pulse Energy (mJ)
Pulse Width (nS)
Temperature (C)
50
40
30
20
10
0
10
9.5
9
8.5
8
7.5
7
6.5
0
5
10
15
20
25
30
35
ba
Q A
'*'

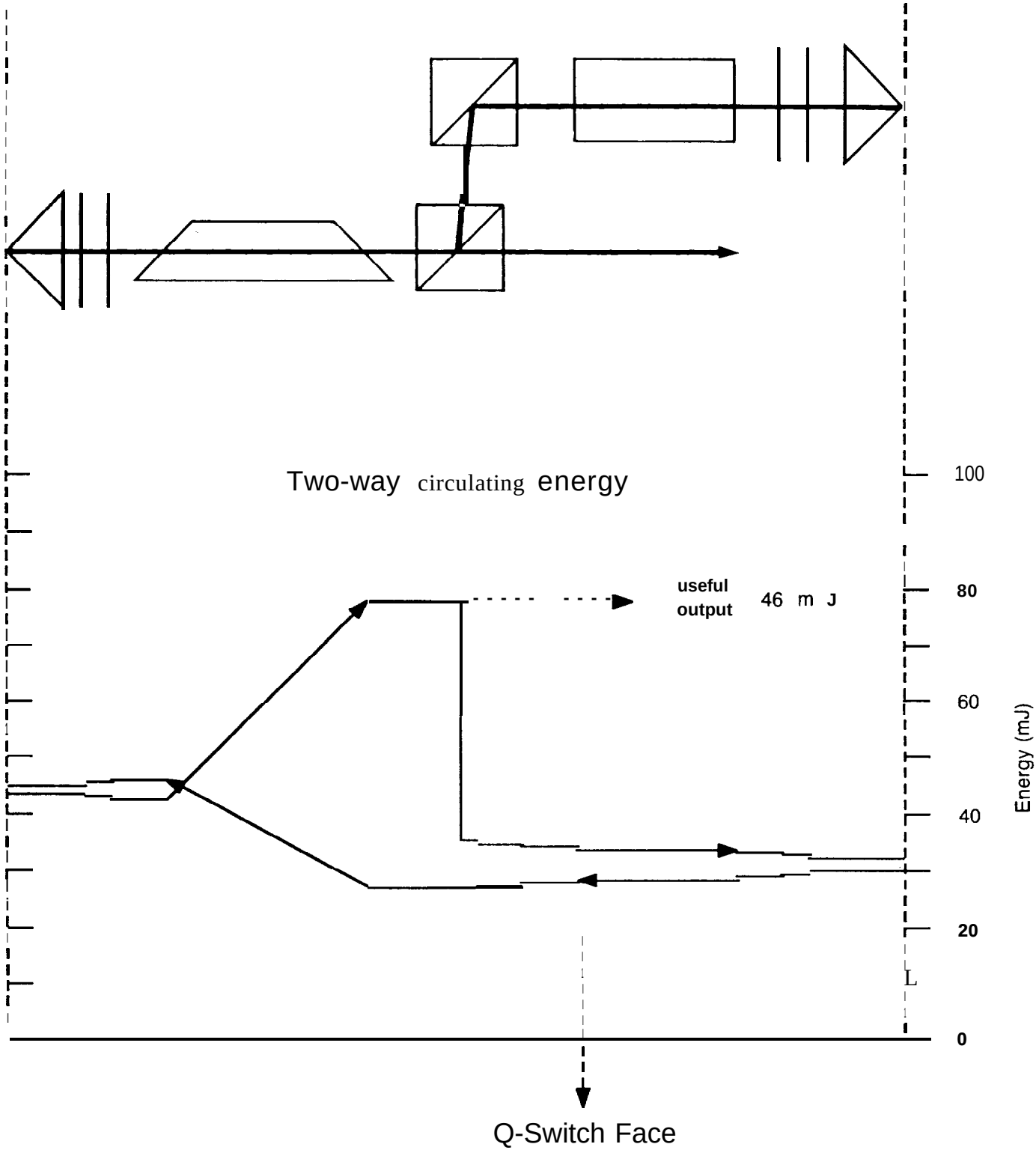
Two-way circulating energy
useful output
46 m J
100
80
60
40
20
0
Energy (mJ)
L
Q-Switch Face